Lagrangian modeling of mass transfer from a single bubble rising in stagnant liquid

Jannike Solsvik

Department of Chemical Engineering, NTNU - Norwegian University of Science and Technology, Trondheim, Norway

E-mail address: jannike.solsvik@chemeng.ntnu.no

Abstract

A Lagrangian model has been derived that describes the size, species composition and velocity of an individual gas bubble as it ascends through a vertical column with stagnant liquid and exchanges mass with the other phase. Various correlations for the liquid-side mass transfer coefficient for laminar flow have been implemented in the Lagrangian model and the predictions are compared with available experimental data in the literature. The predictability of the Lagrangian model is in general not acceptable due to the limitations of the available theoretical framework employed for deriving the existing correlations for the mass transfer coefficient. The various mass transfer coefficients give very different simulation results, and furthermore, the experimental data show a transient behavior in the change of bubble size due to mass transfer which is not captured by the Lagrangian model. An over- or underestimation of the interface mass transfer flux will give an erroneous change of bubble size, which may have significant influence on the predicted bubble rise velocity - in particular if the drag coefficient is very sensitive to the size of the bubble. It is emphasized that the cause of discrepancy between the simulation results and experimental data is not due to the Lagrangian model but mainly caused by the lack of good models for the mass transfer coefficient.

Keywords:

Lagrangian model; mass transfer coefficient; bubbles; interface mass transfer

1 Introduction

Many industrial processes depend on interface gas–liquid mass transfer to or from gas bubbles rising in liquids. Distillation, fermentation, sewage treatment, and chemical reactors such as the bubble column and slurry column are examples. Much research on gas–liquid mass transfer has been performed in bubble swarms and concentrated on the establishment of correlations for the volumetric mass transfer coefficient, $k_L a$. Many physical and mechanical factors contribute to the mass transfer coefficient k_L and the specific bubble surface area a, and their combined effect in the volumetric mass transfer coefficient cannot be easily predicted. To better understand the phenomena involved, researchers have thus suggested to perform the mass transfer experiments of bubble swarms by measuring changes in bulk liquid concentration during which also the average bubble size is determined (Alves et al., 2004; Calderbank and Moo-Yong, 1961; Sardeing et al., 2006). As an alternative to

the experimental study of mass transfer in bubble swarm systems, the phenomena of mass transfer can be studied by performing measurements on individual bubbles in a liquid column. Basically, two experimental approaches have been used in mass transfer experiments of individual bubbles: (i) the bubble is rising in a column with stagnant liquid (Baird and Davidson, 1962; Barnett et al., 1966; Bischof et al., 1991; Calderbank et al., 1970; Calderbank and Lochiel, 1964; Davenport et al., 1967; Deindoerfer and Humphrey, 1961; Garbarini and Tien, 1969; Hosoda et al., 2014; Koide et al., 1976, 1974; Leonard and Houghton, 1963; Mortarjemi and Jameson, 1978; Raymond and Zieminski, 1971; Redfield and Houghton, 1965; Zieminski and Raymond, 1968) and (ii) the bubble is released in a counter-current liquid flow and held stationary by balancing the buoyancy with the downward liquid flow (Alves et al., 2005, 2006; Hosoda et al., 2014; Olsen et al., 2017; Vasconcelos et al., 2002). The second approach is favorable for cases where the mass transfer is slow so that the bubble needs to be monitored over a long time frame (see e.g. Olsen et al., 2017). This work will consider the first approach only. Table 1 provides an overview of the experimental studies in approach (i).

In general, the experimental approaches for mass transfer of single bubbles rising in a column with stagnant liquid are divided into the photographic-, pressure- and concentration based techniques (Bischof et al., 1991; Calderbank and Lochiel, 1964; Deindoerfer and Humphrey, 1961; Garbarini and Tien, 1969). In the photographic methods, the history of bubble size and position as it rises in the column is recorded and the data can be used to compute k_L. For example, the quatities obtained from images for computing k_L in the work by Garbarini and Tien (1969) were bubble volumn, bubble location, their time derivatives, and bubble surface area. In the pressure based techniques, the experimental set-up is designd to allow record of the pressure changes caused by the change in bubble size (Calderbank and Lochiel, 1964). Gas chromatography has been used in the concentration based techniques to determine the change in gas mixture-composition of a gas volume-sample made from bubbles of known size (Bischof et al., 1991).

Most of the single-bubble mass-transfer experiments have determined k_L as function of bubble size and analysed its sensitivity to bubble age and surface-active materials (e.g., Baird and Davidson, 1962; Calderbank and Lochiel, 1964; Deindoerfer and Humphrey, 1961; Koide et al., 1976, 1974). Only a fraction of the limited number of studies on single-bubble mass transfer have compared experimentally determined k_L-values with predictions of theoretical models (Baird and Davidson, 1962; Deindoerfer and Humphrey, 1961; Mortarjemi and Jameson, 1978). Such analyses have been limited to graphs with experimental values for k_L as function of bubble diameter and with one or few theoretical model predictions.

In the present study, a number of theoretical models for k_L have been analyzed using a Lagrangian model description of a single bubble rising in a column with non-flowing liquid. The Lagrangian model predicts the change in bubble volume and – for multicomponent systems – gas mixture composition as it rises through the column due to buoyancy and exposes to the mass transfer phenomenon and the hydrostatic pressure gradient. The numerical results of the Lagrangian model have been compared to experimental data from the literature. The approach of using a Lagrangian model have not previously been employed in such examination of the theoretical models for k_L.

2 Theory and modeling

First, the theoretical concept for interface bubble–liquid mass transfer is presented. Thereafter, a Lagrangian model describing the mass transfer of a bubble rising in stagnant liquid is derived.

2.1 Interface bubble–liquid mass transfer

In figure 1, the liquid- and gas phase are separated by a gas–liquid interface. The volumetric rate of mass transfer of species c from the gas-phase bulk to the gas-side interface is

$$N_{G,c} = k_{G,c}a(C_{G,c} - C_{G,I,c}) \tag{1a}$$

and the volumetric rate of mass transfer of species c from the liquid-side interface to the liquid-phase bulk is

$$N_{L,c} = k_{L,c}a(C_{L,I,c} - C_{L,c}) \tag{1b}$$

At steady state there is no accumulation of species c at the interface. Any species c transported through the liquid-side interface must also be transported through the gas-side interface. Hence, $N_{G,c} = N_{L,c} = N_c$. To avoid problems with determining interface concentrations, the we assume that equilibrium will be attained at the interface:

$$C_{G,I,c} = H_c C_{L,I,c} \tag{2}$$

Relation (2) is substituted into (1a) and (1b):

$$N_c = k_{G,c}a(C_{G,c} - H_c C_{L,I,c}) \tag{3a}$$

$$N_c = k_{L,c}a(\frac{C_{G,I,c}}{H_c} - C_{L,c}) \tag{3b}$$

Equation (1b) is multiplied by H_c and the resulting equation is added to (3a). The result can be written as

$$N_c = \left(\frac{1}{k_{G,c}a} + \frac{H_c}{k_{L,c}a}\right)^{-1}(C_{G,c} - H_c C_{L,c}) = K_{G,c}a(C_{G,c} - H_c C_{L,c}) \tag{4}$$

where the overall mass transfer coefficient $K_{G,c}$ is defined by

$$\frac{1}{K_{G,c}a} = \frac{1}{k_{G,c}a} + \frac{H_c}{k_{L,c}a} \tag{5}$$

Similarly, equation (1a) is multiplied by $1/H_c$ and the resulting equation is added to (3b):

$$N_c = \left(\frac{1}{H_c k_{G,c}a} + \frac{1}{k_{L,c}a}\right)^{-1}\left(\frac{C_{G,c}}{H_c} - C_{L,c}\right) = K_{L,c}a\left(\frac{C_{G,c}}{H_c} - C_{L,c}\right) \tag{6}$$

where the overall mass transfer coefficient $K_{L,c}$ is defined by

$$\frac{1}{K_{L,c}a} = \frac{1}{H_c k_{G,c} a} + \frac{1}{k_{L,c}a} \tag{7}$$

We observe that the interface concentrations have been eliminated from the expressions for N_c in (4) and (6).

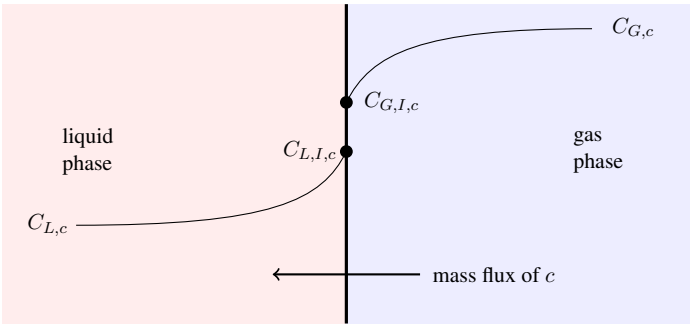

Figure 1: Mass transfer across a gas–liquid interface.

A conventional notation used is to let $H_c C_{L,c}$ in (4) be denoted by $C^*_{G,c}$ and let $C_{G,c}/H_c$ in (6) be denoted by $C^*_{L,c}$. The molar based Henry's law $C_{g,c} = H_c C_{l,c}$ can be expressed in terms of mass density by multiplication with molecular mass on both sides of equality, which yields $\rho_{g,c} = H_c \rho_{l,c}$. If species c is poorly soluble in the liquid, the liquid-phase mass transfer resistance dominates and $k_{G,c}a$ is much larger than $k_{L,c}a$. From relation (7), this means that $K_{L,c}a$ is approximated by $k_{L,c}a$. For the case where species c is largely soluble in the liquid phase so that $k_{L,c}a \gg k_{G,c}a$, $K_{G,c}a$ is approximated by $k_{G,c}a$ from relation (5). Hence, for the case where the main resitance to mass transfer is mainly due to the gas-side interface we have

$$N_c = k_{G,c}a(C_{G,c} - C^*_{G,c}) \tag{8a}$$

Hence, for the cases where the main resistance to mass transfer is mainly due to the liquid-side interface we can write

$$N_c = k_{L,c}a(C^*_{L,c} - C_{L,c}) \tag{8b}$$

Appendix A outlines theoretical concepts for the mass transfer coefficient k_L.

2.2 A Lagrangian model for mass transfer between liquid and a single bubble

A material control volume holds a collection of matter of fixed identity within its control surface. The model framework for analysis of motion of a material control volume is termed Lagrangian. In the following, a Lagrangian model is derived for a single bubble rising in a stagnant liquid column (see figure 2). Here, the bubble–liquid interface defines the surface to the material control volume. The bubble interacts with its surroundings such that the momentum balance of the bubble is influenced by the hydrostatic- pressure-, gravity-, and drag forces. Furthermore, the total mass of the bubble, as well as the species composition in the case of a multi-component system, change due to the mass transfered across the gas–liquid interface. The resulting Lagrangian

model of the single bubble constitutes a set of ordinary differential equations (and closure laws), which in the present work has been solved using the build-in ode15s-solver in MATLAB (2017a). The following model derivation make use of the Leibniz and Gauss theorems which are provided in Appendix B.

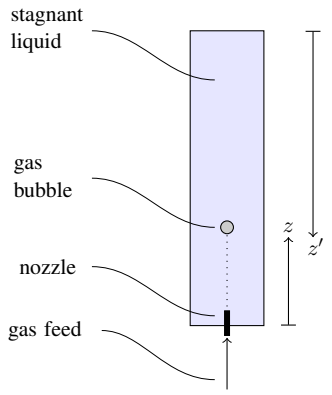

Figure 2: Single bubble rise in a vertical column with stagnant liquid.

2.2.1 Bubble size

In this work, we are interested in the change of bubble size due to hydrostatic pressure and mass transfer across the gas–liquid interface. The size of the bubble can be determined from the total mass balance.

In the Lagrangian model framework, the total mass of a bubble is formulated as

$$m_b(t) = \int\limits_{V_b(t)} \rho_g(\mathbf{r}, t)\,\mathrm{d}v \tag{9}$$

The differentiation of (9) with time is written as

$$\frac{\mathrm{d}m_b}{\mathrm{d}t} = \frac{\mathrm{d}}{\mathrm{d}t}\int\limits_{V_b} \rho_g\,\mathrm{d}v \tag{10}$$

Applying the Leibniz rule to the RHS of (10) results in (Morel, 2015, Eq. 2.66)

$$\frac{\mathrm{d}}{\mathrm{d}t}\int\limits_{V_b(t)} \rho_g\,\mathrm{d}v = \int\limits_{V_b(t)} \frac{\partial \rho_g}{\partial t}\,\mathrm{d}v + \oint\limits_{S_b(t)} \rho_g \mathbf{u}_g \cdot \mathbf{n}_g\,\mathrm{d}s + \oint\limits_{S_b(t)} \rho_g(\mathbf{u}_I - \mathbf{u}_g)\cdot \mathbf{n}_g\,\mathrm{d}s \tag{11}$$

The Gauss theorem is used to rewrite the first surface integral of (11) into a volume integral and the resulting equation is substituted into (10), which results in

$$\frac{\mathrm{d}m_b}{\mathrm{d}t} = \int\limits_{V_b(t)} \left[\frac{\partial \rho_g}{\partial t} + \nabla\cdot(\rho_g \mathbf{u}_g)\right]\mathrm{d}v + \oint\limits_{S_b(t)} \rho_g(\mathbf{u}_I - \mathbf{u}_g)\cdot \mathbf{n}_g\,\mathrm{d}s \tag{12}$$

The conservation principle of mass (13) governs inside the bubble volume, hence the volume integral on the

RHS of (12) vanishes.

$$\frac{\partial \rho_g}{\partial t} + \nabla \cdot (\rho_g \mathbf{u}_g) = 0 \tag{13}$$

Let us define the quantity $\dot{m}$ as the mass *gain* for the bubble per unit surface and time (Morel, 2015, Eg. 2.17):

$$\dot{m} = \rho_g(\mathbf{u}_I - \mathbf{u}_g) \cdot \mathbf{n}_g \tag{14}$$

Here, we model the interface coupling term $\rho_g(\mathbf{u}_I - \mathbf{u}_g) \cdot \mathbf{n}_g$ as (i.e. make a closure law)

$$\rho_g(\mathbf{u}_I - \mathbf{u}_g) \cdot \mathbf{n}_g := \sum_c k_{L,c}(\rho_{l,c} - \rho^*_{l,c}) = \sum_c k_{L,c}(\rho_{l,c} - \rho_{g,c}/H_c) \tag{15}$$

where $\rho^*_{l,c} = \rho_{g,c}/H_c$ assumes a spherical bubble. Table 3 provides the Henry's constant for CO_2, N_2 and O_2 at 298K and 1 atm. With the assumption of an uniform mass transfer condition over the entire bubble surface, we have

$$\oint_{S_b(t)} \dot{m}\, \mathrm{d}s = \dot{m} S_b \tag{16}$$

where $S_b = \pi d_b^2$. In terms of (13), (14) and (16), equation (12) can be written as

$$\frac{\mathrm{d}m_b}{\mathrm{d}t} = \dot{m} S_b \tag{17}$$

Assuming that there is no mass density gradient in the bubble, then the total mass of the bubble is related with the bubble volume through the relation $m_b = \rho_g V_b$. Hence, (17) can be expressed in terms of bubble volume instead of bubble mass as

$$\begin{aligned} &\frac{\mathrm{d}}{\mathrm{d}t}(\rho_g V_b) = V_b \frac{\mathrm{d}\rho_g}{\mathrm{d}t} + \rho_g \frac{\mathrm{d}V_b}{\mathrm{d}t} = \dot{m} S_b \\ &\Rightarrow \frac{\mathrm{d}V_b}{\mathrm{d}t} = -\frac{V_b}{\rho_g}\frac{\mathrm{d}\rho_g}{\mathrm{d}t} + \frac{\dot{m} S_b}{\rho_g} \end{aligned} \tag{18}$$

The bubble is assumed spherical so that the volume and diameter are related by $V_b = (\pi/6) d_b^3$.

Please also consult appendix C.

2.2.2 Bubble velocity

The bubble rise velocity can be determined from the bubble momentum balance. In the Lagrangian framework, the conservation of momentum of the bubble can be written as

$$m_b(t)\mathbf{w}_b(t) = \int_{V_b(t)} \rho_g(\mathbf{r}, t)\mathbf{v}_b(\mathbf{r}, t)\, \mathrm{d}v \tag{19}$$

where $\mathbf{w}_b$ is the center of mass velocity of the bubble. The differentiation of (19) is given as

$$\frac{\mathrm{d}}{\mathrm{d}t}(m_b \mathbf{w}_b) = \frac{\mathrm{d}}{\mathrm{d}t} \int\limits_{V_b(t)} \rho_g \mathbf{v}_b \,\mathrm{d}v \tag{20}$$

Leibniz RHS of (20) (Morel, 2015, Eq. 2.68)

$$\frac{\mathrm{d}}{\mathrm{d}t} \int\limits_{V_b(t)} \rho_g \mathbf{v}_b \,\mathrm{d}v = \int\limits_{V_b(t)} \frac{\partial}{\partial t}(\rho_g \mathbf{u}_g) \,\mathrm{d}v + \oint\limits_{S_b(t)} \rho_g \mathbf{u}_g \mathbf{u}_g \cdot \mathbf{n}_g \,\mathrm{d}s + \oint\limits_{S_b(t)} \rho_g \mathbf{u}_g (\mathbf{u}_I - \mathbf{u}_g) \cdot \mathbf{n}_g \,\mathrm{d}s \tag{21}$$

The Gauss theorem is applied to transform the first surface integral of (21) into a volume integral. Equation (20) can thus be expressed as

$$\frac{\mathrm{d}}{\mathrm{d}t}(m_b \mathbf{w}_b) = \int\limits_{V_b(t)} \left[\frac{\partial}{\partial t}(\rho_g \mathbf{u}_g) + \nabla \cdot (\rho_g \mathbf{u}_g \mathbf{u}_g) \right] \mathrm{d}v + \oint\limits_{S_b(t)} \rho_g \mathbf{u}_g (\mathbf{u}_I - \mathbf{u}_g) \cdot \mathbf{n}_g \,\mathrm{d}s \tag{22}$$

where the surface integral of (22) can be expressed in terms of $\dot{m}$ defined by (14). Furthermore, the equation of momentum (23) governs in the bubble volume, and the LHS of (23) is recognized as the integrand of the volume integral of (22).

$$\frac{\partial}{\partial t}(\rho_g \mathbf{u}_g) + \nabla \cdot (\rho_g \mathbf{u}_g \mathbf{u}_g) = -\nabla \big(p_{\text{hydrostat}} + p_{\text{dyn}} \big) - \nabla \cdot \boldsymbol{\sigma} - \rho_g g \mathbf{e}_z \tag{23}$$

The hydrostatic force is given as (Crowe et al., 1998, sec. 4.3.2)

$$\mathbf{F}_{\text{hydrostat}} = \oint\limits_{S_b(t)} -p_{\text{hydrostat}} \mathbf{n}_g \,\mathrm{d}s = \int\limits_{V_b(t)} -\nabla p_{\text{hydrostat}} \,\mathrm{d}v \tag{24}$$

where the Gauss theorem is used in the latter equality. By assuming the pressure gradient is constant over the bubble volume, (24) simplifies to $\mathbf{F}_{\text{hydrostat}} = -\nabla p_{\text{hydrostat}} V_b$. Furthermore, let the pressure gradient be produced by the hydrostatic pressure, i.e. $\nabla p_{\text{hydrostat}} = -\rho_l g \mathbf{e}_z$, then we obtain

$$\mathbf{F}_{\text{hydrostat}} = \rho_l g V_b \mathbf{e}_z \tag{25}$$

Hence, the force is equal to the weight of liquid displaced by the bubble volume (i.e., the Archimedes principle). The hydrodynamic force is defined by (Jakobsen, 2014, Eq. 5.6)

$$\mathbf{F}_{\text{hydrodyn}} = -\oint\limits_{S_b(t)} \big(p_{\text{dyn}} \mathbf{I} + \boldsymbol{\sigma} \big) \cdot \mathbf{n}_g \,\mathrm{d}s \tag{26}$$

The hydrodynamic force is composed of contributions such as steady drag, history, lift and virtual mass forces (Jakobsen, 2014, Eq. 5.7):

$$\mathbf{F}_{\text{hydrodyn}} = \mathbf{F}_{\text{D}} + \mathbf{F}_{\text{hist}} + \mathbf{F}_{\text{L}} + \mathbf{F}_{\text{V}} \tag{27}$$

Here, we will only consider the steady drag force defined as (Crowe et al., 1998, sec. 4.36)

$$\mathbf{F}_{\mathrm{D}} = \frac{1}{2}\rho_l C_D A_b^p |\mathbf{w}_l - \mathbf{w}_b|(\mathbf{w}_l - \mathbf{w}_b) \tag{28}$$

where $A_b^p = S_b/4$ is the projected area of the bubble. Equation (22) can thus be expressed as

$$\frac{\mathrm{d}}{\mathrm{d}t}(m_b \mathbf{w}_b) = \rho_l g V_b \mathbf{e}_z - m_b g \mathbf{e}_z + \frac{1}{2}\rho_l C_D A_b^p |\mathbf{w}_l - \mathbf{w}_b|(\mathbf{w}_l - \mathbf{w}_b) + \dot{m}\mathbf{u}_g S_b \tag{29}$$

Introducing the assumptions of a stagnant liquid phase, uniform gas velocity in the bubble volume $\mathbf{w}_b = \mathbf{u}_g$, and bubble motion in only the z-direction. Equation (29) can thus be written as

$$\frac{\mathrm{d}}{\mathrm{d}t}(m_b u_{g,z}) = \rho_l g V_b - m_b g - \frac{1}{2}\rho_l C_D A_b^p |u_{g,z}| u_{g,z} + \dot{m} u_{g,z} S_b \tag{30}$$

Table 4 provides the drag correlations proposed by Tomiyama et al. (1998) for bubbles in clean-, partly contaminated-, and contaminated water systems.

2.2.3 Bubble pressure

The Young-Laplace equation gives the phase pressure difference across bubble interface (Probstein, 1994, Eq. 10.1.6):

$$\Delta p = p_g - p_l = \frac{-4\sigma}{d_b} \tag{31}$$

For the bubble-liquid systems of interest in the present study, the interface tension term is negligible compared to the liquid pressure. Hence,

$$p_g = p_l + \frac{-4\sigma}{d_b} \approx p_l \tag{32}$$

2.2.4 Bubble species mass balances

The species mass balance is required if the bubble is composed of a gas mixture. The mass of species c in the bubble is

$$m_{b,c}(t) = \int\limits_{V_b(t)} \rho_{g,c}(\mathbf{r}, t)\,\mathrm{d}v \tag{33}$$

Equation (33) is differentiated with time:

$$\begin{aligned}
\frac{\mathrm{d}m_{b,c}}{\mathrm{d}t} &= \frac{\mathrm{d}}{\mathrm{d}t}\int\limits_{V_b(t)} \rho_{g,c}\,\mathrm{d}v \\
&= \int\limits_{V_b(t)} \frac{\partial \rho_{g,c}}{\partial t}\,\mathrm{d}v + \oint\limits_{S_b(t)} \rho_{g,c}\mathbf{u}_{g,c}\cdot\mathbf{n}_g\,\mathrm{d}s + \oint\limits_{S_b(t)} \rho_{g,c}(\mathbf{u}_I-\mathbf{u}_{g,c})\cdot\mathbf{n}_g\,\mathrm{d}s \\
&= \int\limits_{V_b(t)} \left[\frac{\partial \rho_{g,c}}{\partial t} + \nabla\cdot\left(\rho_{g,c}\mathbf{u}_{g,c}\right)\right]\mathrm{d}v + \oint\limits_{S_b(t)} \rho_{g,c}(\mathbf{u}_I-\mathbf{u}_{g,c})\cdot\mathbf{n}_g\,\mathrm{d}s \\
&= \oint\limits_{S_b(t)} \rho_{g,c}[(\mathbf{u}_I-\mathbf{u}_g)-\mathbf{U}_{g,c}]\cdot\mathbf{n}_g\,\mathrm{d}s \\
&= \oint\limits_{S_b(t)} [\rho_{g,c}(\mathbf{u}_I-\mathbf{u}_g)\cdot\mathbf{n}_g - \mathbf{J}_{g,c}\cdot\mathbf{n}_g]\,\mathrm{d}s
\end{aligned} \tag{34}$$

Here, it is used that $\partial\rho_{g,c}/\partial t + \nabla\cdot\left(\rho_{g,c}\mathbf{u}_g + \mathbf{J}_{g,c}\right) = \partial\rho_{g,c}/\partial t + \nabla\cdot\left(\rho_{g,c}\mathbf{u}_{g,c}\right) = 0$ as there is no chemical reactions in the bubble volume. Furthermore, the species velocity is the sum of mass average velocity and diffusion velocities, i.e. $\mathbf{u}_{g,c} = \mathbf{u}_g + \mathbf{U}_{g,c}$. We continue the derivation by introducing the quantity $\dot{m}_c$ as the mass *gain* of species c for the bubble per unit surface and time (Jakobsen, 2014, Eq. 3.93):

$$\begin{aligned}
\dot{m}_c &= \rho_{g,c}(\mathbf{u}_I-\mathbf{u}_g)\cdot\mathbf{n}_g - \mathbf{J}_{g,c}\cdot\mathbf{n}_g \\
&= k_{L,c}\left(\rho_{l,c}-\rho^*_{l,c}\right) = k_{L,c}\left(\rho_{l,c}-\rho_{g,c}/H_c\right)
\end{aligned} \tag{35}$$

where (see Eq. 14)

$$\dot{m} = \sum_c \dot{m}_c \tag{36}$$

Hence, equation (34) can be written as

$$\frac{\mathrm{d}m_{b,c}}{\mathrm{d}t} = \dot{m}_c S_b \tag{37}$$

The latter equation can alternatively be rewritten using the relation $m_{b,c} = V_b\rho_g\omega_{g,c}$:

$$\begin{aligned}
&\frac{\mathrm{d}}{\mathrm{d}t}\left(V_b\rho_g\omega_{g,c}\right) = V_b\rho_g\frac{\mathrm{d}\omega_{g,c}}{\mathrm{d}t} + \omega_{g,c}\frac{\mathrm{d}}{\mathrm{d}t}\left(V_b\rho_g\right) = \dot{m}_c S_b \\
&\Rightarrow \frac{\mathrm{d}\omega_{g,c}}{\mathrm{d}t} = \frac{\dot{m}_c S_b}{V_b\rho_g} - \frac{\omega_{g,c}\dot{m}S_b}{V_b\rho_g}
\end{aligned} \tag{38}$$

where (18) has been used.

2.2.5 Liquid phase pressure

The momentum equation of the liquid phase is deduced from the gross-scale averaged Euler-Euler model (Jakobsen, 2014, Eq. 3.502):

$$-\alpha_l \frac{\mathrm{d}p_l}{\mathrm{d}z} + \alpha_l g_z \rho_l = 0 \tag{39}$$

where $\alpha_l \approx 1$. Equation (39) is integrated:

$$p_l(z) = p_a + g\rho_l(L - z) \tag{40}$$

where $p_a = p_l(z = L)$ is the atmospheric pressure.

2.2.6 Liquid phase species mass balances

We assume that the change in the liquid phase composition is negligible during the mass transfer process of a single rising bubble. Hence a constant value for $\rho_l \omega_{l,c}$ is specified for the system.

2.2.7 Other relations

The ideal gas law $m_b R T_g = V_b \bar{M}_g p_g$ is differentiated as follows (for constant temperature system)

$$\frac{\mathrm{d}\rho_g}{\mathrm{d}t} = \frac{\mathrm{d}}{\mathrm{d}t}\left(\frac{\bar{M}_g p_g}{R T_g}\right) = \frac{\bar{M}_g}{R T_g}\frac{\mathrm{d}p_g}{\mathrm{d}t} + \frac{p_g}{R T_g}\frac{\mathrm{d}\bar{M}_g}{\mathrm{d}t} \tag{41}$$

The derivative $\mathrm{d}z/\mathrm{d}t$ is identified as the instantaneous bubble velocity (Garbarini and Tien, 1969):

$$\frac{\mathrm{d}z}{\mathrm{d}t} = u_g \tag{42}$$

Hence, equation (42) is used to relate the velocity of the rising bubble with its position in the liquid column. Expressions for the derivatives $\mathrm{d}p_g/\mathrm{d}t$ and $\mathrm{d}\bar{M}_g/\mathrm{d}t$ on the RHS of (41) are given as, respectively (Deindoerfer and Humphrey, 1961)

$$\frac{\mathrm{d}p_g}{\mathrm{d}t} = \frac{\mathrm{d}}{\mathrm{d}t}\big(p_a + g\rho_l[L - z(t)]\big) = -g\rho_l\frac{\mathrm{d}z}{\mathrm{d}t} = -g\rho_l u_g \tag{43}$$

(where (40) and (42) are used) and

$$\frac{\mathrm{d}\bar{M}_g}{\mathrm{d}t} = \sum_c M_c \frac{\mathrm{d}\omega_{g,c}}{\mathrm{d}t} \tag{44}$$

The following dimensionless groups are used in the present modeling study. The bubble Reynolds number gives the ratio between the inertial resistance to viscous resistance for a flowing fluid:

$$\mathrm{Re} = \frac{\rho_l |u_{\mathrm{rel}}| d_b}{\mu_l} \tag{45}$$

The Schmidt number is defined as the ratio of momentum diffusivity (kinematic viscoisty) and mass diffusivity:

$$\mathrm{Sc} = \frac{\mu_l}{\rho_l D} \tag{46}$$

The Eötvös number gives the ratio between the gravitational and surface tension forces:

$$\mathrm{Eo} = \frac{(\rho_l - \rho_b) g d_b^2}{\sigma} \tag{47}$$

The Galilei number gives the gravitational over viscous forces:

$$\mathrm{Ga} = \frac{\rho_l^2 g d_b^3}{\mu_l^2} \tag{48}$$

The Grashof number is the ratio of buoyancy to viscous force (Calderbank and Moo-Yong, 1961):

$$\mathrm{Gr} = \frac{d_b^3 \rho_l \Delta\rho g}{\mu_l^2} \tag{49}$$

The Sherwood number is expressed in terms of the mass transfer coefficient as

$$\mathrm{Sh} = \frac{k_L d_b}{D} \tag{50}$$

In mass transfer problems, the Sherwood number often depends on dimensionless groups such as the Reynolds number and Schmidt number; $\mathrm{Sh} = \phi(\mathrm{Re}, \mathrm{Sc})$, the Galilei number and Schmidt number; $\mathrm{Sh} = \phi(\mathrm{Ga}, \mathrm{Sc})$, or the Grashof number and Schmidt number; $\mathrm{Sh} = \phi(\mathrm{Gr}, \mathrm{Sc})$ (see Table 5).

2.2.8 Model assumptions

The experiments by Garbarini and Tien (1969) and Deindoerfer and Humphrey (1961) consider bubbles of pure CO_2-gas. In both of these experiments it is assumed that the CO_2-concentration in the liquid-phase is negligible. The liquid was degassed in the work by Garbarini and Tien (1969), hence the balance of mass in the Lagrangian model is limited to the total continuity equation only. Deindoerfer and Humphrey (1961) saturated the liquid with helium before the bubbles was injected, hence a consistent Lagrangian model should include species mass balances for CO_2 and helium. In addition to mass transfer of CO_2 from bubble to liquid, helium might also be transferred from liquid to bubble. It is reasonable to assume that the concentration of helium in the liquid is equal to the maximum concentration of helium that can be dissolved.

The experiment by Bischof et al. (1991) considers a binary gas mixture of oxygen and nitrogen (air bubbles). In this case the Lagrangian model must include the species mass balances for these components. The liquid was saturated with nitrogen before the bubbles were injected, hence the liquid concentration of nitrogen in the Lagrangian model was set equal to the maximum concentration of nitrogen that can be dissolved in the medium. Furthermore, it is assumed that the oxygen content in the liquid-phase can be neglected compared to that in the gas-phase.

3 Results and discussion

3.1 Mass transfer correlations

Both bubble rise velocity and interface mass transfer between bubble and surrounding liquid depend on water purity. According to Olsen et al. (2017), only distilled water usually qualifies as a *clean* condition. *Contaminated* water may contain surface-active components; known as surfactants, which affect (i.e. reduce) the bubble surface mobility. The intermediate impurity condition is commonly referred to as *partly contaminated*.

The bubble Reynolds number is required in the k_L-correlations (Tab. 5) by Higbie (1935) (K1), Frössling (1938) (K2), Hughmark (1967) (K5), Brauer (1979) (K7), Bird et al. (1960) (K8), and Clift et al. (1978) (K9). On the other hand, the k_L-correlations by Calderbank and Moo-Yong (1961) (K3), Baird and Davidson (1962) (K4), and Clift et al. (1978) (K6) do not depend on the bubble Reynold number and consequently the prediction of interface mass transfer flux by these models is insensitive to the bubble hydrodynamics (i.e. bubble rise velocity). The correlations for mass transfer listed in Tab. 5 are plotted in Figure 3 as function of bubble diameter. In particular, for correlations K1, K2, K5, and K7–K9, which depends on the bubbly hydrodynamics, the bubble Reynolds number (45) is computed from the terminal bubble velocity obtained from Eq. (51) with the Tomiyama et al. (1998) drag coefficient for (i) clean water and (ii) contaminated water (D1 and D3 in Tab. 4, respectively). Partly contaminated water (drag coefficient D2 in Tab. 4) is not shown in Figure 3 but the k_L-correlations K1, K2, K5, and K7–K9 takes values in between the limits of (i) and (ii) (notice the similar terminal velocity of clean and partly contaminated condition in Figure 8).

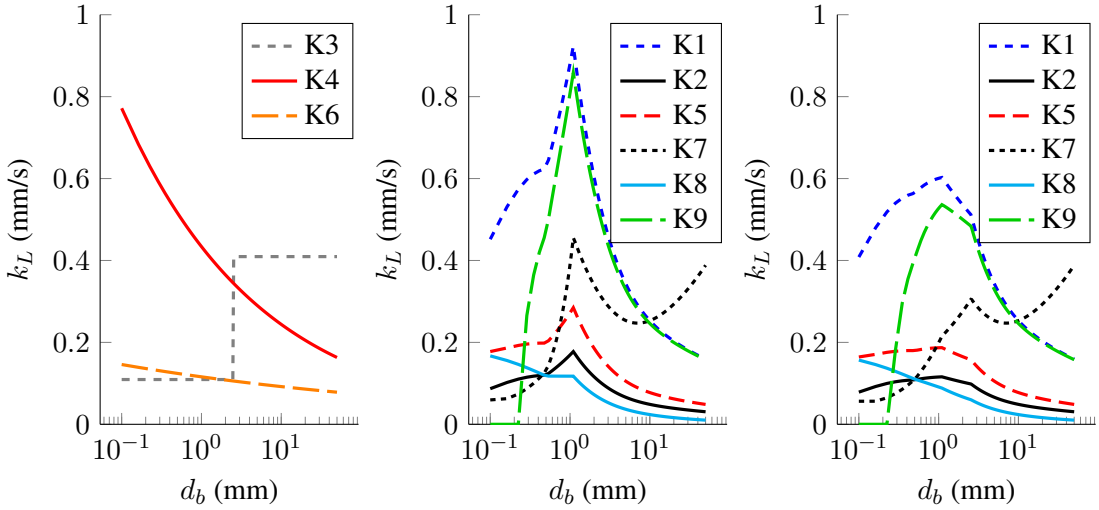

Figure 3: Plot of the mass transfer correlations in Tab. 5. k_L-correlations independent of Reynolds number (left), terminal velocity and drag coefficient for clean system (middle), and terminal velocity and drag coefficient for contaminated system (right).

The k_L-coefficient is a function of bubble rigidity. The upper values of k_L occur for a bubble with a totally mobile surface (i.e. clean condition) and the lower values of k_L occur for a bubble with totally rigid surface (i.e. contaminated condition) (Alves et al., 2005). In partly contaminated conditions, small bubbles will behave

as bubbles with a rigid interface and large bubbles will behave as bubbles with a mobile interface (Olsen et al., 2017). This phenomena occurs because the impurities are present in relatively small concentrations such that fast rising bubbles; which are typically the large bubbles, are able to shed the surrounding layer of contaminated conditions and thus keep the interface relatively mobile (Olsen et al., 2017).

The k_L-correlation by Higbie (1935) is derived for totally mobile interfaces (i.e. clean condition) (Alves et al., 2005). This coincide with Figure 3 where K1 predicts an upper limit among the plotted k_L-correlations. A consistent implementation of the Lagrangian model should therefor combine the Higbie (1935) (K1) correlation with the drag coefficient for clean systems (i.e. D1 in Tab. 4).

From Figure 3, the k_L-correlations by Calderbank and Moo-Yong (1961) (K3), Brauer (1979) (K7) and Clift et al. (1978) (K9) predict lower k_L-values for smaller bubbles and higher k_L-values for larger bubbles. These k_L-correlations are thus suitable for partly contaminated conditions. Correlations K3, K7 and K9 should be combined with the drag coefficient for partly contaminated system (i.e. D2 in Tab. 4) to obtain a consistent Lagrangian model.

Frössling (1938) derived a k_L-correlation for rigid interfaces (i.e. contaminated conditions) (Alves et al., 2004). From Figure 3 we observe that K2 predicts a lower value for the mass transfer coefficient. Similar predictions of the k_L-value is obtained with the k_L-correlations by Hughmark (1967) (K5), Clift et al. (1978) (K6) and Bird et al. (1960) (K8). A consistent Lagrangian model should thus combine the drag coefficient for contaminated conditions (D3 in Tab. 4) with either K2, K5, K6, or K8.

The k_L-correlation by Baird and Davidson (1962) (K4) is strictly valid only for bubble diameters in between 14 and 73 mm. The range of validity of K4 explains its different prediction of the k_L-coefficient compared to the other k_L-correlations for the smaller bubble sizes in Figure 3.

There is a general trend in Figure 3 that those models with a dependency as $\mathrm{Sc}^{1/2}$ apply to free-slip on the bubble surface, i.e. clean systems, whilst those models with a dependency as $\mathrm{Sc}^{1/3}$ apply to no-slip on the bubble surface, i.e. interface with impurities (i.e. partly- and contaminated conditions). See also Tables 5 and 6.

The discussion above is summarized in Table 6.

3.2 Lagrangian model prediction versus experimental data

The numerical solution of the Lagrangian model presented previously has been compared with available sets of experimental data for individual bubbles exposed to mass transfer as they rise in a column with stagnant liquid.

3.2.1 Experimental data by Bischof et al. (1991)

Bischof et al. (1991) studied mass transfer from individual air bubbles into water of different quality. The bubbles were released at the bottom of a column and collected at different heights in a diver and the gas composition was analyzed by gas chromatography. Before the bubbles were fed into the column, the liquid was deoxygenated by aerating the column with nitrogen such that the liquid was completely saturated with nitrogen. Hence, in addition to mass transfer of oxygen from the bubble into the liquid, there may have also been mass transfer of nitrogen from the liquid into the bubble as the nitrogen concentration in the water is very high compared to that inside the bubble.

The relative amount of oxygen transferred from an air bubble to the liquid (distilled water) is shown in figure 4 for two bubble sizes: 0.9 and 2.0 mm. It is observed from the experimental data of Bischof et al. (1991) that the mass transfer flux of oxygen depends on the initial bubble size for the two size classes presented. We also notice that the correlations for the mass transfer coefficient k_L in table 5 depend on the bubble size (see also Fig. 3). The k_L-correlations listed in table 5 are implemented in the present Lagrangian model and compared to the experimental data. In general, the various k_L-correlations give very different predictions of the mass transfer phenomena. For the smaller initial bubble size, the k_L-correlations by Baird and Davidson (1962) (K4) and Brauer (1979) (K7) predict the experimental data best. For the larger initial bubble size, the best model prediction is obtained with the k_L-correlations by Higbie (1935) (K1) and Clift et al. (1978) (K9). For the smaller initial bubble size, the model predictions with the various k_L-correlations are in the range of about 20–80% transferred oxygen from the bubble when it reaches the top of the column, while it is in the range of 5–35% for the larger initial bubble size. The experimental values are 42% and 38%, respectively.

In figure 5, bubbles with initial diameter of 1.3 mm are analyzed in liquids of different quality. Figure 5 shows that the liquid purity (distilled- and waste water) influences significantly on the amount of transferred oxygen from bubble to liquid. Among the k_L-correlations in table 5, the best model prediction in the case of distilled water is obtained with the correlations by Higbie (1935) (K1) and Clift et al. (1978, Eq. 5-37) (K9), and the correlation by Hughmark (1967) (K5) gives the best model prediction in the case of waste water. These simulation results are in agreement with the textcolorMyColorpreviously discussed classification of the k_L-correlations according to clean, partly contaminated and contaminated systems (see Fig. 3). We also notice that the best model prediction of the mass transfer experiments for 1.3 mm initial bubble diameter (Fig. 5) and 2 mm initial bubble diameter (Fig. 4) in distilled water, are obtained with the K1-correlation for fully mobile bubble interface and the K9-correlation for partly contaminated system. On the other hand, for 0.9 mm initial bubble diameter in distilled water (Fig. 4), the K1-correlation significantly over-predicts the mass transfer process. This observation is surprising considering that the same water quality (i.e. distilled) is expected in both the experimental runs with the 0.9 and 2 mm initial diameter bubbles.

The k_L-correlation by Baird and Davidson (1962) (K4) predicts the mass transfer process well for the 0.9 mm initial bubble diameter in Figure 4. This is surprising considering that this k_L-correlation is developed for large bubble diameters (i.e. 14–73 mm). Furthermore, K4 shows an increasing value of the k_L-coefficient with decreasing bubble size (see Fig. 3) which is contradictory to the behavior of the other k_L-correlations and also in conflict with the generally accepted literature that smaller bubbles are rigid which reduces the k_L-coefficient (Doran, 2013).

There is a significant limitation in the experimental data set provided by Bischof et al. (1991) for proper validation of the present Lagrangian model due to the fact that the k_L-correlations quantifies how fast species are moving across an interface. That is, in these experiments the amount of oxygen transferred from the bubble to the liquid is only given as function of position in the vertical column. The total mass of oxygen transferred from the bubble to the liquid is not only determined by the total mass transferred but also affected by the residence time of the bubble in the liquid (i.e. bubble rise velocity). Information on the time taken for a bubble to rise through the vertical liquid column, i.e., the position of bubble in the column as function of time, is required in order to analyze the bubble hydrodynamics which determines the available time for mass to move across the

interface during the experiments. This time consideration of single bubble mass transfer experiments is included in the data sets provided by Garbarini and Tien (1969) and Deindoerfer and Humphrey (1961) discussed in the following.

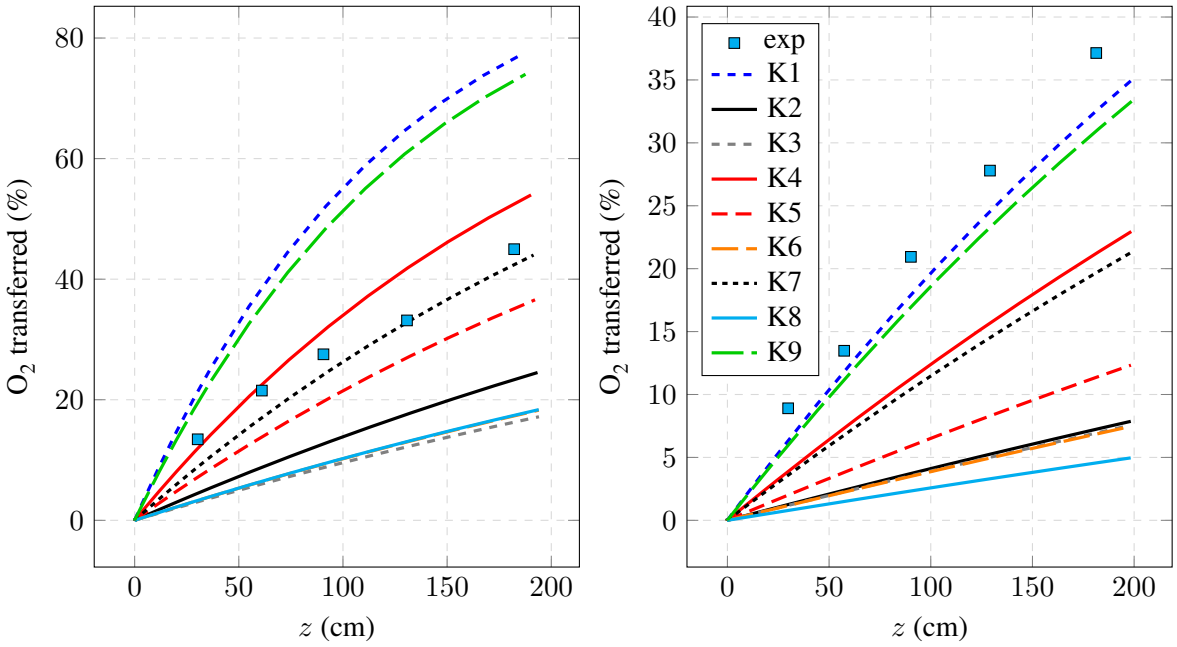

Figure 4: O_2 transferred from a bubble with initial bubble diameters of 0.9 mm (left) and 2 mm (right) in distilled water. Experimental data by Bischof et al. (1991, Fig. 5). Left figure: K6 and K8 (and K3) overlap. Right figure: K2, K3 and K6 overlap.

3.2.2 Experimental data by Garbarini and Tien (1969)

Garbarini and Tien (1969) investigated mass transfer from single CO_2 bubbles rising through degassed water. Both photographic- and pressure based methods were analyzed.

In figure 6, the change of bubble size (with initial diameter of 5.2 mm) is given along with the information on bubble position in the vertical column as well as the time taken from the release of the bubble. Here, a representative selection of the k_L-correlations in table 5 is presented. The experimental data for the change in the bubble diameter shows a significant larger gradient the first second after the bubble release. This dynamic is not captured by the Lagrangian model, which predicts a linear reduction of the bubble diameter with time. The effect of bubble age on experimentally determined k_L-values are discussed in the literature (Alves et al., 2004; Deindoerfer and Humphrey, 1961) but remains to be further elaborated.

There are large differences in the predicted bubble diameter at the outlet of the vertical column, i.e. between 0 and 4.8 mm, for the various k_L-correlations analyzed, while it is 2.45 mm in the experimental measurement (see fig. 6). Although there are significant differences in the predicted bubble size by the Lagrangian model as shown in Fig. 6, the variations have minor influence on the bubble rise velocity. Figure 6 shows that the Lagrangian model prediction of the vertical bubble position with time agrees very well with the experimental

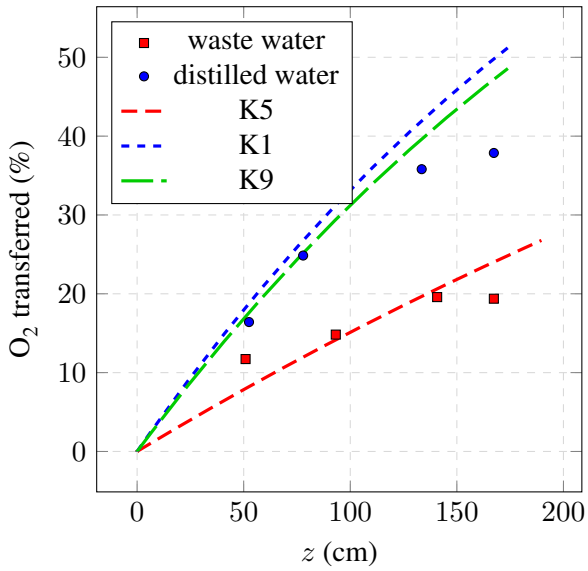

Figure 5: O_2 transferred from a bubble with initial bubble diameter of 1.3 mm in distilled and waste water. Experimental data by Bischof et al. (1991, Fig. 6).

data.

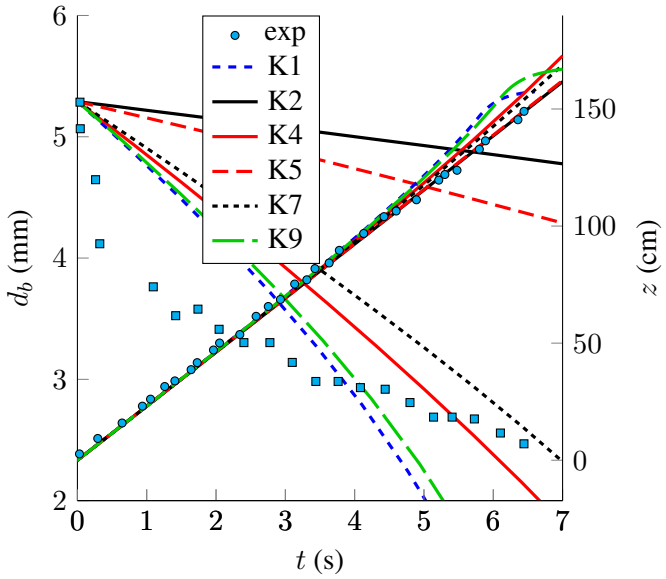

Figure 6: Change in size and axial position for a CO_2-bubble rising in stagnant distilled water. (Garbarini and Tien, 1969, Figs. 4 and 5).

3.2.3 Experimental data by Deindoerfer and Humphrey (1961)

Deindoerfer and Humphrey (1961) designed the equipment to permit determination of bubble size and liquid

head by photographing a single CO_2 gas bubble as it ascended through a vertical column filled with water. The sketch of the experimental set-up indicated that the water was saturated with helium before the bubble experiments, hence the measured bubble size might have been influenced by mass transfer of helium from the liquid phase to the gas phase. However, as the solubility of helium is low, i.e. 0.0015 gram helium per kg water at 25 degree Celsius, the predictions of the mass transfer process by the Lagrangian model showed minor differences between the two cases of completely degassed water and water saturated with helium.

Deindoerfer and Humphrey (1961) did not provide any information on the quality of the water used in their mass transfer experiments. Hence, the drag coefficient by Tomiyama et al. (1998) for both clean and contaminated systems were implemented in the Lagrangian model and analyzed.

Figure 7 shows that the changes in bubble size and bubble liquid head with time can be fairly predicted only the first two seconds after the bubble is released in the water. In contrast to the results in figure 6 (Garbarini and Tien, 1969), there are significant deviations between the Lagrangian model predictions and experimental data for the vertical bubble position in the column. An explanation for this can be given based on figure 8. Here, the drag coefficient correlations by Tomiyama et al. (1998) (tab. 4) are plotted along with the resulting terminal velocities. The terminal velocities plotted in figure 8 are computed from force balances including gravity, buoyancy and drag, which results in (Olsen et al., 2017)

$$u_t = [4gd_b(\rho_l - \rho_g)/(3C_D\rho_l)]^{(1/2)} \tag{51}$$

The terminal velocity of this equation is obtained in an iterative manner together with the expression for drag coefficient (see table 4). In figure 7, the experimental bubble diameter is 2.7 mm at the release point and it reduces to 1.2 mm at the top of the vertical column. Figure 8 reveals that there are significant gradients in the drag coefficients and terminal velocities for this bubble size range. In contrast, such large gradients are not present for larger bubble diameters such as in the case of figure 6 (Garbarini and Tien, 1969) which give better agreement with the experimental data for the bubble rise velocity.

Figure 7 (Deindoerfer and Humphrey, 1961) supports the observation made previously in figure 6 (Garbarini and Tien, 1969) that there are in general week agreements between experimental data for bubble size and Lagrangian model predictions. Furthermore, also for this case the various k_L-correlations implemented in the Lagrangian model give very different predictions of the experimental data.

3.2.4 Dynamic trend in the data by Garbarini and Tien (1969) and Deindoerfer and Humphrey (1961)

In both the experimental data by Garbarini and Tien (1969) and Deindoerfer and Humphrey (1961) there is a dynamic trend in the bubble size as function of time, i.e. there is a greater gradient of bubble size reduction just after bubble injection than it is observed for the bubble when it has traveled further up in the water column. None of the k_L-correlations in Table 5 capture this dynamics. The k_L-coefficient strongly depends on whether contaminants are present or not (see Fig. 5).

According to the discussion by Alves et al. (2004), experiments have shown that a bubble surface may be free of surfactants when formed but its behavior changes in time as contaminants accumulate at the interface,

and this may explain why k_L depends on time. These authors also point out that larger bubbles remain mobile for a longer period, because they are slower to accumulate enough impurities for transition to rigidity and may be a reason why larger bubbles tend to be mobile while smaller bubbles tend to be rigid. Alves et al. (2005) highlighted that there exist few experimental studies on the simultaneous decrease in mass transfer and terminal velocity as a bubble gets contaminated.

Although distilled water (and thus presumable contaminated-free system) was used in the experiments by Garbarini and Tien (1969), the effect of accumulation of contaminates on the bubble surface (as discussed by Alves et al. (2004)) seems to have taken place in these experiments. In this context, it is interesting to note that the bubble-size data by Garbarini and Tien (1969) in Figure 6 for times larger than one second have about the same gradient as the k_L-correlations K2 (Frössling, 1938) and K5 (Hughmark, 1967) for rigid bubbles, or contaminated conditions. On the other hand, for the initial times less than one second, none of the k_L-correlations for nor clean, partly-contaminated or contaminaded conditions capture the slope of the bubble-size change. In the experiments by Deindoerfer and Humphrey (1961) provided in Figure 7, the k_L-correlation by Brauer (1979) (K7) capture the gradient of the bubble-size change the first four seconds after bubble release. The K7-correlation is for partly contaminated conditions. The bubble size change after four seconds has about the same gradient as that of the k_L-correlations by Bird et al. (1960) (K8) for contaminated systems, but with a different starting point for the bubble size.

3.2.5 The Lagrangian model

The interface mass transfer process is complex and affected by time and space dependent key factors such as interface diffusion and convection, surrounding flow field of the bubble, interface impurities, as well as bubble surface deformations. For a bubble rising in a stagnant liquid, the conditions for mass transfer may differ significantly between the top and bottom regions of the bubble surface.

In the Lagrangian model, a set of ordinary differential equations are used to describe the evolution of bubble volume, bubble rise velocity, and species composition of the bubble in a multicomponent system. The phenomena taking place in the mass transfer process between the bubble and surrounding liquid is lumped into the k_L-coefficient, which is the governing parameter when estimating the mass transfer rate. Furthermore, the bubble dynamics is described in terms of interface forces such as the drag force.

The present study shows that the correlations for k_L predicts the interface mass transfer insufficiently even in the case where the bubble hydrodynamics (i.e. bubble rise velocity) is accurately captured by the model. The Lagrangian model provides a sufficiently accurate mathematical framework to draw the conclusion that there are severe limitations of the k_L-correlations (for prediction of the present experimental data). The complexity of the mass transfer process discussed in the start of Section 3.2.5, is not well lumped into the k_L-coefficient.

4 Concluding remarks

This paper presents a Lagrangian model of a single bubble rising in a vertical column with stagnant liquid. The bubble size changes as the bubble ascends along its vertical path due to hydrostatic pressure and mass exchange between the two phases. An important parameter in the Lagrangian model is the liquid-side mass

transfer coefficient k_L in the interface mass flux term. When implementing various k_L-correlations for laminar flow and analyze the results of the Lagrangian model, not acceptable predictions of experimental data available in the literature are obtained. It is know from existing literature that the proposed k_L-correlations may give very different predictions. However, it is surprising that the existing correlations for k_L cannot be used to predict the simplest experimental flow situation denoting an individual bubble rising in a stagnant liquid with interface mass transfer. One may make a critical statement to the available theoretical framework employed for deriving the existing correlations for the mass transfer coefficient. The drag coefficient is identified as another critical parameter in the Lagrangian model. For the experimental data available in the literature, it is, however, more crucial for the Lagrangian model prediction that improved correlations for k_L are developed. That is, for a particular data set (Garbarini and Tien, 1969) the Lagrangian model predicted very well the bubble hydrodynamics (i.e. rise velocity), but the mass transfer flux deviated significantly from that of the experimental

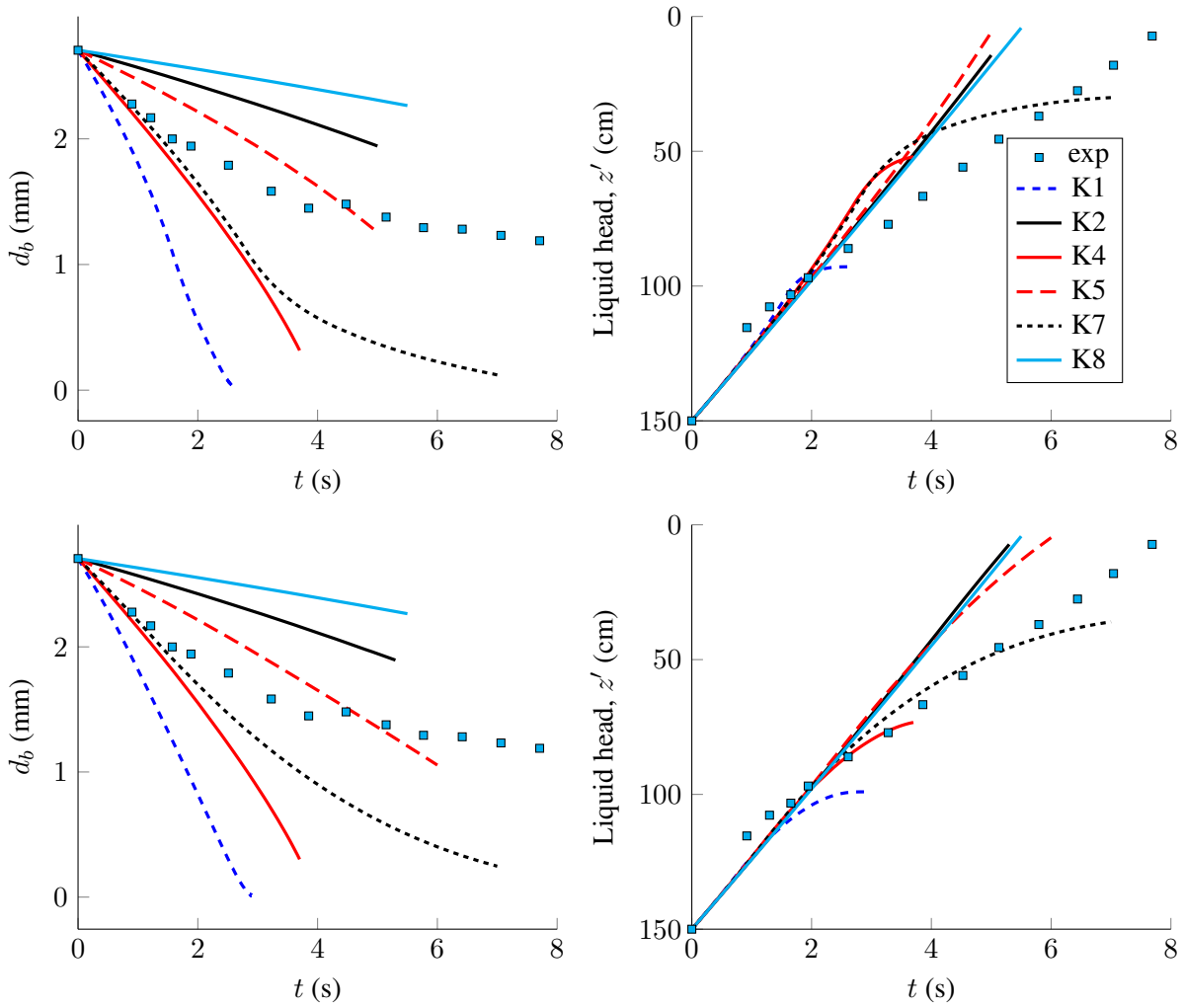

Figure 7: Change in bubble size (left) and liquid head of bubble (right) with time (Deindoerfer and Humphrey, 1961, Fig. 1). Drag coefficients by Tomiyama et al. (1998) for clean- (top) and contaminated (bottom) systems are implemented in the Lagrangian model.

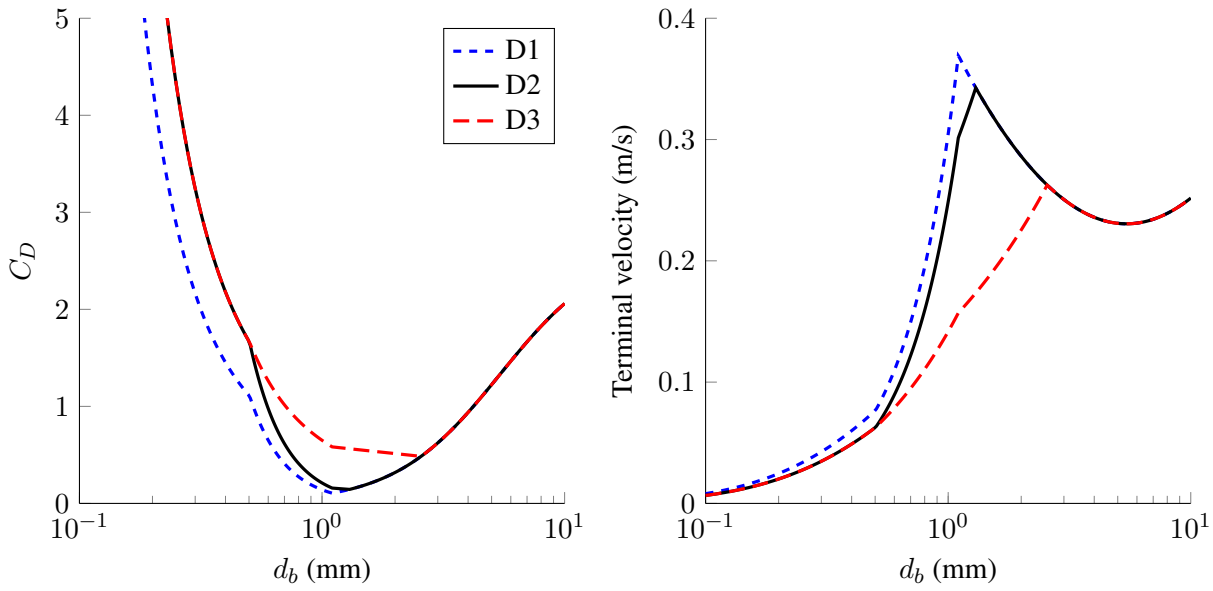

Figure 8: Drag correlation (left) proposed by Tomiyama et al. (1998) and its predicted terminal velocity (right) for clean- (D1), partly contaminated- (D2), and contaminated (D3) systems. For physical conditions see Tab. 2.

results.

The existing experimental data on mass transfer from individual bubbles rising in a stagnant liquid are old and not extensive. For the present study, data sets from three studies in the 60's and early 90's could be used to evaluate the present Lagrangian model (Bischof et al., 1991; Deindoerfer and Humphrey, 1961; Garbarini and Tien, 1969). One may rise doubt about the accuracy of these data sets as the statistics of experiments are hardly discussed. Furthermore, because of the water quality has a pronounce influence on bubble rigidity, it is also important that experimental data are provided along with details on the water contamination. As significant technological developments have taken place the last few years, there is a significant potential for new studies to provide new and extensive sets of experimental data with higher accuracy.

The experimental data by Garbarini and Tien (1969) and Deindoerfer and Humphrey (1961) appear to be influenced by contaminants in the way that the interface is mobile at bubble release but contaminants accumulate with time and make the interface rigid as it rise through the water column. The general trend is that k_L-correlations for clean or partly contaminated conditions best describe the bubble size change the first time after bubble release, thereafter the gradient in the bubble size can be better captured with the k_L-correlations for contaminated systems. Further research needs to account for the absorption kinetics of contaminates or experiments need to be devised and implemented carefully to exclude the effect of accumulating contaminates at the interface.

The present study conclude that the cause of discrepancy between experimental data and simulation results is not due to the Lagrangian model, but mainly caused by the lack of good models for the k_L-coefficient.

It is crucial to understand the fundamental principles of interface mass transfer in simple systems such as single bubbles rising in a stagnant liquid before more complex systems including for example turbulent flow can

be understood. The present Lagrangian model serves as a good tool for validation of k_L-correlations for laminar flow. However, new model developments for k_L must be supported with new and extensive sets of experimental data.

References

Alves, S. S., Maia, C. I., Vasconcelos, J. M. T., 2004. Gas–liquid mass transfer coefficient in stirred tank interpreted through bubble contamination kinetics. Chem. Eng. Process. 43, 823–830.

Alves, S. S., Orvalho, S. P., Vasconcelos, J. M. T., 2005. Effect of bubble contamination on rise velocity and mass transfer. Chem. Eng. Sci. 60, 1–9.

Alves, S. S., Vasconcelos, J. M. T., Orvalho, S. P., 2006. Mass transfer to clean bubbles at low turbulent energy dissipation. Chem. Eng. Sci. 61, 1334–1337.

Baird, M. H. I., Davidson, J. F., 1962. Gas absorption by large rising bubbles. Chem. Eng. Sci. 17, 87–93.

Barnett, S. M., Humphrey, A. E., Litt, M., 1966. Bubble motion and mass transfer in non-Newtonian fluids. AIChE J. 12, 253–259.

Bird, R. B., Stewart, W. E., Lightfoot, E. N., 1960. Transport phenomena. Wiley, New York.

Bischof, F., Sommerfeld, M., Durst, F., 1991. The determination of mass transfer rates from individual small bubbles. Chem. Eng. Sci. 46, 3115–3121.

Brauer, H., 1979. Particle/fluid transport processes. Fortschritte der Verfahrenstechnik 17, 61–99.

Calderbank, P. H., Johnson, D. S. L., Loudon, J., 1970. Mechanics and mass transfer of single bubbles in free rise through some Newtonian and non-Newtonian liquids. Chem. Eng. Sci. 25, 235–256.

Calderbank, P. H., Lochiel, A. C., 1964. Mass transfer coefficients, velocities and shapes of carbon dioxide bubbles in free rise through distilled water. Chem. Eng. Sci. 19, 485–503.

Calderbank, P. H., Moo-Yong, M. B., 1961. The continuous phase heat and mass-transfer properties of dispersions. Chem. Eng. Sci. 16, 39–54.

Clift, R., Grace, J. R., Weber, M. E., 1978. Bubbles, drops, and particles. Academic Press, San Diego.

Crowe, C., Sommerfeld, M., Tsuji, Y., 1998. Multiphase flows with droplets and particles. CRC Press, Boca Raton.

Danckwerts, P. V., 1951. Significance of liquid-film coefficients in gas absorption. Ind. Eng. Chem. Res. 43, 1460–1467.

Davenport, W. G., Richardson, F. D., Bradshaw, A. V., 1967. Spherical cap bubbles in low density liquids. Chem. Eng. Sci. 22, 1221–1235.

Deindoerfer, F. H., Humphrey, A. E., 1961. Mass transfer from individual gas bubbles. Ind. Eng. Chem. 53, 755–759.

Doran, P. M., 2013. Bioprocess engineering principles. Academic Press, Amsterdam.

Frössling, N., 1938. Über die verdunstung falender tropfen. Beitr Geophys. 52, 170–216.

Garbarini, G. R., Tien, C., 1969. Mass transfer from single gas bubble – A comparative study on experimental methods. Can. J. Chem. Eng. 47, 35–41.

Higbie, R., 1935. The rate of absorption of a pure gas into a still liquid during a short time of exposure. Transactions of the American Institute of Chemical Engineers 31, 365–389.

Hines, A. L., Massox, R. N., 1985. Mass transfer: Fundamentals and applications. Prentice Hall PTR, Englewoods Cliffs, New Jersey.

Hosoda, S., Abe, S., Hosokawa, S., Tomiyama, A., 2014. Mass transfer from a bubble in a vertical pipe. Int. J. Heat Mass Transfer 69, 215–222.

Hughmark, G. A., 1967. Liquid–liquid spray column drop size, holdup and continuous phase mass transfer. I&EC Funda. 58, 107–114.

Jakobsen, H. A., 2014. Chemical reactor modeling: Multiphase reactive flows, 2nd Edition. Vol. 1. Springer, Berlin.

Koide, K., Hayashi, T., Sumino, K., Iwamoto, S., 1976. Mass transfer from single bubbles in aqueous solutions of surfactants. Chem. Eng. Sci. 31, 963–967.

Koide, K., Orito, Y., Hara, Y., 1974. Mass transfer from single bubbles in Newtonian liquids. Chem. Eng. Sci. 29, 417–425.

Leonard, J. H., Houghton, G., 1963. Mass transfer and velocity of rise phenomena for single bubbles. Chem. Eng. Sci. 18, 133–142.

Morel, C., 2015. Mathematical modeling of dispersed two-phase flows. Springer, Heidelberg.

Mortarjemi, M., Jameson, G. J., 1978. Mass transfer from very small bubbles–The optimum bubble size for aeration. Chem. Eng. Sci. 33, 1415–1423.

Olsen, J. E., Dunnebier, D., Davies, E., Skjetne, P., Morud, J., 2017. Mass transfer between bubbles and seawater. Chem. Eng. Sci. 161, 308–315.

Probstein, R. F., 1994. Physicochemical hydrodynamics. An Introduction, 2nd Edition. John Wiley & Sons, New York.

Raymond, D. R., Zieminski, S. A., 1971. Mass transfer and drag coefficient of bubbles rising in dilute aqueous solutions. AIChE J. 17, 57–65.

Redfield, J. A., Houghton, G., 1965. Mass transfer and drag coefficient for single bubbles at Reynolds numbers of 0.02–5000. Chem. Eng. Sci. 20, 131–139.

Rousseau, W. R., 1987. Handbook of separation process technology. John Wiley & Sons, New York.

Sardeing, R., Painmanakul, P., Hebrard, G., 2006. Effect of surfactants on liquid-side mass transfer coefficient in gas–liquid systems: A first step to modeling. Chem. Eng. Sci. 61, 6249–6260.

Tomiyama, A., Kataoka, I., Zun, I., Sakaguchi, T., 1998. Drag coefficient of single bubbles under normal and micro gravity conditions. JSME Int. J. Ser. B 41, 472–479.

Vasconcelos, J. M. T., Orvalho, S. P., Alves, S. S., 2002. Gas–liquid mass transfer to single bubbles: Effect of surface contamination. AIChE J. 48, 1145–1154.

Zieminski, S. A., Raymond, D. R., 1968. Experimental study of the bahavior of single bubbles. Chem. Eng. Sci. 23, 17–28.

Table 1: Experimental mass transfer studies of single bubbles rising in a column with stagnant liquid.

Reference	Comments
Deindoerfer and Humphrey (1961)	k_L determined by photographic measurement technique; CO_2 and water; 1mm$<d_b<$6mm influence of bubble age on mass transfer; time-dependent factors are important in mass transfer
Baird and Davidson (1962)	$k_L$determined by photographic measurement technique; CO_2 in water; effect of surface-active agents; 8mm$<d_b<$42mm; influence of bubble age on mass transfer
Leonard and Houghton (1963)	He, C_2H_4, N_2 and N_2O gases; 3mm$<d_b<$19mm, dilatometric and photoelectric determination of mass transfer
Calderbank and Lochiel (1964)	CO_2; 4mm$<d_b<$31mm; large bubbles; the effect of the instantaneous shape of the bubble on the instantaneous transfer coefficient; k_L determined by pressure measurement technique
Redfield and Houghton (1965)	CO_2 in water and 10 different aqueous solutions of dextrose providing ranges of viscosity and density variations; 5mm$<d_b<$16mm; dilatometric and photoelectric determination of mass transfer
Barnett et al. (1966)	CO_2; non-Newtonian liquid (CMC solution); 1.5mm$<d_b<$4.5mm; photographic technique measuring technique for determining k_L; role of bubble-shape transition versus non-Newtonian character
Zieminski and Raymond (1968)	2.6mm$<d_b<$5.6mm; CO_2 and water; k_L determined by photographic measurement technique; effect of the bubble release time on the consistency of the k_L-value
Garbarini and Tien (1969)	CO_2 and water; 3mm$<d_b<$6mm; comparison between pressure measurement technique and photographic measurement technique for determining k_L
Calderbank et al. (1970)	CO_2; Newtonian and non-Newtonian liquids; 2mm$<d_b<$60mm; k_L determined by pressure measurement technique
Raymond and Zieminski (1971)	CO_2 and water; alcohol solutions; k_L determined by photographic measurement technique; 3mm$<d_b<$4mm; alcohol solutions have a pronounced effect on mass transfer as well as drag coefficient of the rising bubble
Koide et al. (1974)	CO_2; 4.6mm$<d_b<$8.5mm; water and aqueous solutions of n-propanol, i-butanol, acetic acid and n-octanol; k_L determined by pressure measuring technique; effect of bubble age on k_L
Koide et al. (1976)	5.2mm$<d_b<$10.2mm; CO_2; water and aqueous solutions of n-hexanol, n-heptanol and n-octanol; effect of surface-active chemicals on k_L; k_L determined by pressure measuring technique

Mortarjemi and Jameson (1978)	oxygen and water; 0.2mm$<$ d_b $<$2mm; k_L determined by photographic technique; optimal bubble diameter for oxygen transfer
Bischof et al. (1991)	air bubbles in water; gas chromatography; fraction oxygen transfered to liquid; 0.5mm$<$ d_b $<$2.3mm;
Hosoda et al. (2014)	5mm$<$ d_b $<$26mm; CO_2 and water; stereoscopic image processing; various tube diameters of bubble rising column

Table 2: Physical conditions used for the generation of Figs. 8 and 3.

ρ_g	kg/m^3	2
ρ_l	kg/m^3	998
μ_l	kg/(m·s)	8.91×10^{-4}
D	m^2/s	2×10^{-9}
σ	N/m	0.072

Table 3: Henry's constant and molecular diffusivity at 298K and 1 atm.

Component	$H_c \cdot 10^2$ [m^3·Pa/mol]	$D_c \cdot 10^{-9}$ [m^2/s]
CO_2	29	1.92
N_2	1562.5	2.01
O_2	769	2.10
He	2700	6.28

The term $H_c\rho_g/(M_cP_g)$ is dimensionless.

Table 4: Drag coefficient correlations.

Model	Reference	C_D	Comment
D1	Tomiyama et al. (1998)	$\max\left\{\min\left[\frac{16}{\mathrm{Re}}\left(1+0.15\mathrm{Re}^{0.687}\right), \frac{48}{\mathrm{Re}}\right], \frac{8}{3}\frac{\mathrm{Eo}}{\mathrm{Eo}+4}\right\}$	clean
D2	Tomiyama et al. (1998)	$\max\left\{\min\left[\frac{24}{\mathrm{Re}}\left(1+0.15\mathrm{Re}^{0.687}\right), \frac{72}{\mathrm{Re}}\right], \frac{8}{3}\frac{\mathrm{Eo}}{\mathrm{Eo}+4}\right\}$	partly contaminated
D3	Tomiyama et al. (1998)	$\max\left\{\frac{24}{\mathrm{Re}}\left(1+0.15\mathrm{Re}^{0.687}\right), \frac{8}{3}\frac{\mathrm{Eo}}{\mathrm{Eo}+4}\right\}$	contaminated

Table 5: Correlations for the mass transfer coefficient in laminar flow.

Model	Reference	k_L [m/s]	Bubble diameter range
K1	Higbie (1935)	$2\pi^{-1/2}\mathrm{Re}^{1/2}\mathrm{Sc}^{1/2}(D/d_b)$	
K2	Frössling (1938)	$0.6\mathrm{Re}^{1/2}\mathrm{Sc}^{1/3}(D/d_b)$	
K3a	Calderbank and Moo-Yong (1961)	$0.31\mathrm{Gr}^{1/3}\mathrm{Sc}^{1/3}(D/d_b)$	$d_b < 2.5$mm
K3b	Calderbank and Moo-Yong (1961)	$0.42\mathrm{Gr}^{1/3}\mathrm{Sc}^{1/2}(D/d_b)$	$d_b > 2.5$mm
K4	Baird and Davidson (1962)	$0.975\mathrm{Ga}^{1/4}\mathrm{Sc}^{1/2}(D/d_b)$	14mm$< d_b <$ 73mm
K5	Hughmark (1967)	$\left(2+0.95\mathrm{Re}^{1/2}\mathrm{Sc}^{1/3}\right)(D/d_b)$	
K6	Clift et al. (1978, Eq. 5-26)	$0.45\mathrm{Gr}^{0.3}\mathrm{Sc}^{1/3}(D/d)$	$d_b > 0.1$mm
K7	Brauer (1979)	$(2+0.015\mathrm{Re}^{0.89}\mathrm{Sc}^{0.7})(D/d_b)$	
K8	Bird et al. (1960)	$\left(4+1.21\mathrm{Re}^{2/3}\mathrm{Sc}^{2/3}\right)^{1/2}(D/d_b)$	
K9	Clift et al. (1978, Eq. 5-37)	$2\pi^{-1/2}\left(1-2.89/\max\left[2.89,\sqrt{\mathrm{Re}}\right]\right)^{1/2}\mathrm{Re}^{1/2}\mathrm{Sc}^{1/2}(D/d_b)$	

The liquid diffusivity, D, for CO_2, N_2, O_2 and He are provided in table 3

Table 6: Comments to the correlations for mass transfer.

Model	Reference	Comments
K1	Higbie (1935)	Penetration theory
		Mobile bubble surface
		Clean system
		Dependency $Sc^{1/2}$
K2	Frössling (1938)	Boundary layer theory
		Rigid bubble
		Contaminated system
		Dependency $Sc^{1/3}$
		Experimental values of coefficient vary from 0.42 to 0.95 (Alves et al., 2004)
K3a	Calderbank and Moo-Yong (1961)	Empirical
		Small, rigid bubbles
		Partly contaminated system
		Dependency $Sc^{1/3}$
K3b	Calderbank and Moo-Yong (1961)	Empirical
		Large, non-rigid bubbles
		Partly contaminated system
		Dependency $Sc^{1/2}$
K4	Baird and Davidson (1962)	Spherical cap bubbles
		Fitted model in wobbling regime
		Coefficient between 0.93 and 0.99
		Dependency $Sc^{1/2}$
K5	Hughmark (1967)	Contaminated system (Olsen et al., 2017)
		Dependency $Sc^{1/3}$
K6	Clift et al. (1978, Eq. 5-26)	Rigid spheres
		Fitted model
		Contaminated system
		Dependency $Sc^{1/3}$
K7	Brauer (1979)	Fitted model between numerical and experimental data
		Nonspherical bubbles with stochastic deformation of interface
		Partly contaminated system
K8	Bird et al. (1960)	Contaminated system (Olsen et al., 2017)
		Dependency $Sc^{1/3}$
K9	Clift et al. (1978, Eq. 5-37)	Partly contaminated (Olsen et al., 2017)
		Dependency $Sc^{1/2}$
		Penetration theory
		Fluid spheres

Notation

Latin letters

a	interfacial area per unit volume, m^{-1}
d	diameter, m
$\mathbf{e}$	unit vector
f	generalized function
$\mathbf{f}$	generalized vector or tensor
$\mathbf{F}$	force, N
g	gravity, m/s^2
k	mass transfer coefficient, m/s
l	film thickness, m
m	mass, kg
$\dot{m}$	mass flux, kg/s·m^2
$\mathbf{n}$	unit normal vector
p	pressure, Pa
$\mathbf{r}$	coordinate, vector, m
t	time, s
$\mathbf{u}$	velocity vector, m/s
$\mathbf{w}$	center of mass velocity vector, m/s
z	height from bottom of column, m
z'	axial dimension, length from liquid column surface, m
A	area or surface, m^2
C	concentration, mol/m^3
C_D	drag coefficient
D	diffusivity, m^2/s
H	Henry's constant,
$\mathbf{I}$	unit tensor
K	overall mass transfer coefficient, m/s
L	length of column/height of water, m
$\bar{M}$	average molecular weight,
N	rate of mass transfer, mol/s·m^3
R	gas constant,
S	surface, m^2
T	temperature, K
U_c	diffusion velocity of species c, m/s
V	volume, m^3
Eo	Eötvös number
Gr	Grashof number
Ga	Galilei number

Re	Reynolds number
Sc	Schmidt number
Sh	Sherwood number
Greek Letters	
α_k	volume fraction of phase k
β	Bunsen absorption coefficient
ρ	density, kg/m^3
σ	interface tension, N/m
$\boldsymbol{\sigma}$	viscous stress tensor, Pa
τ	average exposure time of fluid element, s
γ	prefactor
ϕ	generalized function
μ	viscosity, kg/(m·s)
Subscripts	
b	bubble
c	species type
g	gas phase
l	liquid phase
k	phase
t	terminal
z	coordinate, vector component
G	gas phase
I	interface
L	liquid phase
D	steady drag
L	lift
V	virtual mass
dyn	dynamic
hist	history
hydrodyn	hydrodynamic
hydrostat	hydrostatic
rel	relative
Superscripts	
$*$	concentrations with Henry's constant
p	projected

A Theoretical model consepts for the mass transfer coefficient k_L

A.1 Film theory

Fig. 9 illustrates the concept of the film theory (Jakobsen, 2014). A stagnant film of thickness $l = l_l + l_g$ exists near the phase interface and all resistance to mass transfer across the phase interface resides in the film. Concentration gradients occur only in the film whereas the concentrations at length l_l and l_g from the phase interface is equal to the bulk concentrations in the liquid and gas phases, respectively. The mass transfer flux across the film is described as a steady diffusion flux. Within this steady-state process the mass flux is constant as the concentration profile is linear and independent of the diffusion coefficient.

Based on the film theory, the following relations can be derived between the mass transfer- and diffusion coefficients (Jakobsen, 2014):

$$k_{L,c} = \frac{D_{L,c}}{l_l} \qquad \text{and} \qquad k_{G,c} = \frac{D_{G,c}}{l_l} \tag{A.1}$$

Hence, the result obtained from the film theory is that the mass transfer coefficient is directly proportional to the diffusion coefficient. In terms of the Sherwood number $\mathrm{Sh} = kl/D$, the relations in (A.1) can be expressed as

$$\frac{k_{L,c} l_l}{D_{L,c}} = \mathrm{Sh} = 1 \qquad \text{and} \qquad \frac{k_{G,c} l_g}{D_{G,c}} = \mathrm{Sh} = 1 \tag{A.2}$$

Hence, the film theory can be expressed as $\mathrm{Sh} = 1$.

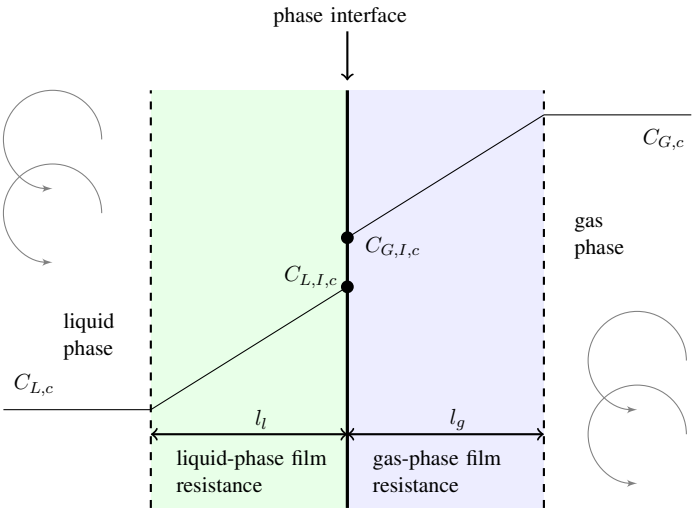

Figure 9: Film theory.

A.2 Penetration theory

The concept of a stagnant film as assumed in the film theory is unrealistic on the basis of the unstableness of a gas–liquid interface (Hines and Massox, 1985). The penetration theory was suggested by Higbie (1935) for more accurate description of the physical process taking place in interfacial mass transfer.

Figure 10 illustrates the concept of the penetration theory (Jakobsen, 2014). Small fluid elements in the liquid phase form discrete entities having certain characteristic flow properties. The fluid elements arrive from the bulk liquid and after residing in contact with the gas phase at the phase interface for a period of time (exposure time) they are replaced and mixed with the bulk liquid again. During the exposure time mass exchange between the fluid element in the liquid phase with the gas phase due to diffusion processes. For short contact times, the diffusion process will be unsteady. It is assumed that the exposure time is equal for all fluid elements. Furthermore, the bulk of both the liquid and gas phases are assumed well mixed.

Based on the penetration theory, the mass transfer coefficient is proportional to square root of the diffusion coefficient:

$$k = 2\sqrt{\frac{D}{\pi t_e}} \tag{A.3}$$

The exposure time of the fluid element, t_e is a fitting parameter into which details of the fluid dynamics are lumped (Jakobsen, 2014).

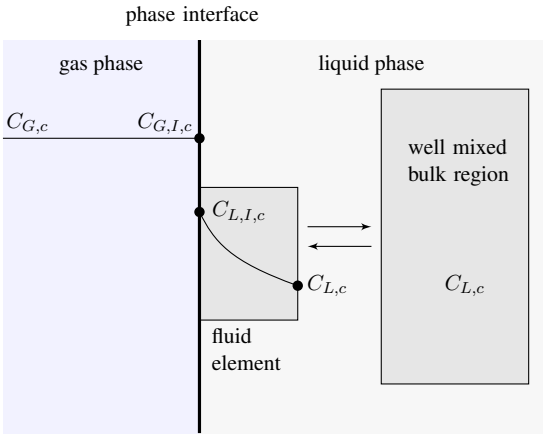

Figure 10: Penetration theory.

A.3 Surface renewal theory

Danckwerts (1951) suggested to improved the penetration theory by replacing the constant exposure time t_e with an average exposure time τ determined from a postulated time distribution. The relation between interfacial mass transfer- and diffusion coefficient can be expressed as (Hines and Massox, 1985; Jakobsen, 2014)

$$k = \sqrt{\frac{D}{\tau}} = \sqrt{Ds} \tag{A.4}$$

where $s = 1/\tau$ is the rate of surface renewal. The surface renewal theory intends to provide a better description of the physical process taking place in interfacial mass transfer. However, the mass transfer coefficient holds the same dependency on the diffusion coefficient. Furthermore, as in the penetration theory, the surface renewal theory depends upon an unknown fitting parameter.

A.4 Mass transfer to the surface of a sphere

Steady-state molecular diffusion to the surface of a sphere in a stagnant fluid can be described by (Clift et al., 1978; Rousseau, 1987)

$$\mathrm{Sh} = \frac{kd}{D} = 2 \tag{A.5}$$

For creeping flow, a laminar boundary layer exists about the sphere. Based on the boundary layer theory it can be shown that the mass transport coefficient can be expressed as a function of the Reynolds number and the Schmidt number: $\mathrm{Sh} = f(\mathrm{Re}, \mathrm{Sc})$. For laminar boundary layer the correlation can be given as (Jakobsen, 2014)

$$\mathrm{Sh} = \gamma \mathrm{Re}^m \mathrm{Sc}^n \tag{A.6}$$

At low flow rates, the correlation for mass transfer is of a form that assumes contributions of molecular diffusion and forced convection are additive (Rousseau, 1987):

$$\mathrm{Sh} = 2 + \gamma \mathrm{Re}^m \mathrm{Sc}^n \tag{A.7}$$

B Theorems

B.1 Leibniz theorems

The Leibniz integral theorem gives a formula for differentiation of an integral whose limits are functions of the differential variable. One of the forms of the Leibniz theorem can be written as (Jakobsen, 2014, Eq. A.8)

$$\frac{\mathrm{D}}{\mathrm{D}t} \int\limits_{V(t)} f(\mathbf{r}, t)\, \mathrm{d}v = \int\limits_{V(t)} \frac{\partial f}{\partial t}\, \mathrm{d}v + \int\limits_{A(t)} f \mathbf{u} \cdot \mathbf{n}\, \mathrm{d}a \tag{B.1}$$

Here we notice the operator $\mathrm{D}/\mathrm{D}t$ which indicates that the velocity $\mathbf{u}$ corresponds to the fluid velocity with respect to the coordinate reference frame. The generalized Leibniz theorem, or the generalized transport theorem, is given as (Jakobsen, 2014, Eq. A.9)

$$\frac{\mathrm{d}}{\mathrm{d}t} \int\limits_{V(t)} f(\mathbf{r}, t)\, \mathrm{d}v = \int\limits_{V(t)} \frac{\partial f}{\partial t}\, \mathrm{d}v + \int\limits_{A(t)} f \mathbf{u} \cdot \mathbf{n}\, \mathrm{d}a \tag{B.2a}$$

Here, the interpretation of $\mathbf{u}$ is the velocity of the control volume surface with respect to the coordinate reference frame. Equation (B.2a) can also be formulated for a vector $\mathbf{f}$ as follows

$$\frac{\mathrm{d}}{\mathrm{d}t} \int\limits_{V(t)} \mathbf{f}(\mathbf{r}, t)\, \mathrm{d}v = \int\limits_{V(t)} \frac{\partial \mathbf{f}}{\partial t}\, \mathrm{d}v + \int\limits_{A(t)} \mathbf{f}\mathbf{u} \cdot \mathbf{n}\, \mathrm{d}a \tag{B.2b}$$

The Leibniz theorem for a surface integral is given as (Morel, 2015, Eq. B.10)

$$\frac{\mathrm{d}}{\mathrm{d}t}\int\limits_{A_I(t)} \rho_I \,\mathrm{d}a = \int\limits_{A_I(t)} \left(\frac{\mathrm{D}_I\rho_I}{\mathrm{D}t} + \rho_I \nabla_I \cdot \mathbf{u}_I\right) \mathrm{d}a \tag{B.3}$$

B.2 Gauss theorems

The Gauss theorem enables a surface integral to be transformed into a volume integral Jakobsen2014. Let $\mathbf{f}$ denote a generalized vector or tensor. The Gauss theorem for single phase is given as

$$\oint\limits_{A(t)} \mathbf{f}\cdot\mathbf{n}\,\mathrm{d}a = \int\limits_{V(t)} \nabla\cdot\mathbf{f}\,\mathrm{d}v \tag{B.4}$$

For two phase flows the interface must be considered and a modified form of the theorem (B.4) is applied:

$$\int\limits_{A_k(t)} \mathbf{f}\cdot\mathbf{n}\,\mathrm{d}a + \int\limits_{A_I(t)} \mathbf{f}\cdot\mathbf{n}\,\mathrm{d}a = \int\limits_{V_k(t)} \nabla\cdot\mathbf{f}\,\mathrm{d}v \tag{B.5}$$

C Two-phase mass balance equation

A two-phase volume is depicted in Figure 11. If we assume this volume to be a material volume, it always contains the same mass during time. Mathematically, a two-phase material volume can be written as

$$\frac{\mathrm{d}}{\mathrm{d}t}\int\limits_{V_1(t)} \rho_1 \,\mathrm{d}v + \frac{\mathrm{d}}{\mathrm{d}t}\int\limits_{V_2(t)} \rho_2 \,\mathrm{d}v + \frac{\mathrm{d}}{\mathrm{d}t}\int\limits_{A_I(t)} \rho_I \,\mathrm{d}a = 0 \tag{C.1}$$

Here, $\rho_k(\mathbf{r},t)$ denotes the density field of phase $k = 1,2$ and $\rho_I(\mathbf{r},t)$ is the interface density field. Using the Leibniz rules (B.2a) for the volume integrals and (B.3) for the surface integral, (C.1) can be rewritten into (Morel, 2015, Eq. 2.13)

$$\begin{aligned}\int\limits_{V_1(t)} \frac{\partial\rho_1}{\partial t}\,\mathrm{d}v + \int\limits_{A_1(t)\cup A_I(t)} \rho_1\mathbf{u}_1\cdot\mathbf{n}_1\,\mathrm{d}a + \int\limits_{V_2(t)} \frac{\partial\rho_2}{\partial t}\,\mathrm{d}v + \int\limits_{A_1(t)\cup A_I(t)} \rho_2\mathbf{u}_2\cdot\mathbf{n}_2\,\mathrm{d}a \\ + \int\limits_{A_I(t)} \left[\rho_1(\mathbf{u}_I-\mathbf{u}_1)\cdot\mathbf{n}_1 + \rho_2(\mathbf{u}_I-\mathbf{u}_2)\cdot\mathbf{n}_2\right]\mathrm{d}a + \int\limits_{A_I(t)} \left(\frac{\mathrm{D}_I\rho_I}{\mathrm{D}t} + \rho_I\nabla_I\cdot\mathbf{u}_I\right)\mathrm{d}a = 0\end{aligned} \tag{C.2}$$

The surface integrals in (C.2) are rewritten into volume integrals using the Gauss theorem (B.5) (Morel, 2015, Eq. 2.14):

$$\begin{aligned}\int\limits_{V_1(t)} \left[\frac{\partial\rho_1}{\partial t} + \nabla\cdot(\rho_1\mathbf{u}_1)\right]\mathrm{d}v + \int\limits_{V_2(t)} \left[\frac{\partial\rho_2}{\partial t} + \nabla\cdot(\rho_2\mathbf{u}_2)\right]\mathrm{d}v \\ + \int\limits_{A_I(t)} \left[\left\{\rho_1(\mathbf{u}_I-\mathbf{u}_1)\cdot\mathbf{n}_1 + \rho_2(\mathbf{u}_I-\mathbf{u}_2)\cdot\mathbf{n}_2\right\} + \left(\frac{\mathrm{D}_I\rho_I}{\mathrm{D}t} + \rho_I\nabla_I\cdot\mathbf{u}_I\right)\right]\mathrm{d}a = 0\end{aligned} \tag{C.3}$$

The balance (C.3) must be satisfied for any V_1, V_2 and A_I, thus the integrands of the volume and surface integrals must all independently be equal to zero. Hence, for a local point occupied by phase k we have

$$\frac{\partial \rho_k}{\partial t} + \nabla \cdot \left(\rho_k \mathbf{u}_k\right) = 0 \tag{C.4}$$

Furthermore, the equation (C.3) gives rise to the following interfacial balance:

$$\sum_{k=1,2} \rho_k (\mathbf{u}_I - \mathbf{u}_k) \cdot \mathbf{n}_k = \frac{\mathrm{D}_I \rho_I}{\mathrm{D}t} + \rho_I \nabla_I \cdot \mathbf{u}_I \tag{C.5}$$

In major applications, mass accumulation on the interface is neglected:

$$\frac{\mathrm{D}_I \rho_I}{\mathrm{D}t} + \rho_I \nabla_I \cdot \mathbf{u}_I = \frac{\partial \rho_I}{\partial t} + \mathbf{v}_I \cdot \nabla_I \rho_I + \rho_I \nabla_I \cdot \mathbf{u}_I = \frac{\partial \rho_I}{\partial t} + \nabla_I \cdot (\rho_I \mathbf{u}_I) = 0 \tag{C.6}$$

Hence,

$$\sum_{k=1,2} \rho_k (\mathbf{u}_I - \mathbf{u}_k) \cdot \mathbf{n}_k = 0 \tag{C.7}$$

where $\rho_k (\mathbf{u}_I - \mathbf{u}_k) \cdot \mathbf{n}_k$ means the mass gain for phase k.

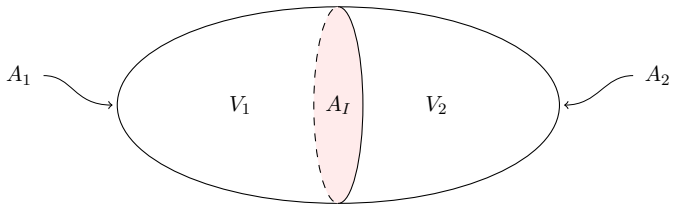

Figure 11: A two-phase volume.